JOURNAL OF MATERIALS SCIENCE **37** (2002) 2407 – 2411

Effect of Fe_2O_3 doping on the electrical properties of a SnO_2 based varistor

A. C. ANTUNES, S. R. M. ANTUNES, A. J. ZARA, S. A. PIANARO
Centro Interdisciplinar de Pesquisa e Pós Graduação - Laboratório Interdisciplinar de Materiais Cerâmicos (LIMAC)- Universidade Estadual de Ponta Grossa, 84031-510 Ponta Grossa, PR, Brazil

E. LONGO
Departamento de Química, UFSCar, 13565-905 São Carlos, SP, Brazil
E-mail: dels@power.ufscar.br

J. A. VARELA
Instituto de Química, UNESP, 14801-970 Araraquara, SP, Brazil

The effect of Fe_2O_3 addition on the densification and electrical properties of the $(0.9895 - x)$ $SnO_2 + 0.01CoO + 0.005Nb_2O_5 + xFe_2O_3$ system, where $x = 0.005$ or 0.01, was considered in this study. The samples were sintered at 1300°C for 2 h. Microstructure analysis by scanning electron microscopy showed that the effect of Fe_2O_3 addition is to decrease the SnO_2 grain size. $J \times E$ curves indicated that the system exhibit a varistor behavior and the effect of Fe_2O_3 is to increase both, the non-linear coefficient (α) and the breakdown voltage (E_r). Considering the Schottky thermionic emission model the potential height and width were estimated. Small amount addition of Fe_2O_3 to the basic system increases both the potential barrier height and width.

1. Introduction

Tin dioxide (SnO_2) is a *n* type wide band gap semiconductor with crystalline structure of rutile type and has low densification rate due to its high surface diffusion at low temperature and high SnO_2 partial pressure at high temperatures [1–3]. Recently, CoO addition to the SnO_2 was observed to lead to 98.5% of theoretical density and made possible the application of these systems in the preparation of varistors [4]. The introduction of either Nb_2O_5 or Ta_2O_5 to the $SnO_2 \cdot CoO$ system decreases the grain resistance, making possible the measurement of breakdown electrical field of these systems [4–7]. The non-linearity of SnO_2 based varistor is strongly influenced by the additions of transition metal oxides such as Cr_2O_3, Bi_2O_3 and MnO_2 [7, 8].

The electric behavior of varistors is governed by the presence of voltage barriers at the grain boundaries [9, 10]. For a given varistor system each voltage barrier is characterized by a specific value v_b. Considering the SnO_2 varistor microstructure, a Schottky type electrical barrier can be ascribed to be most likely barrier at the SnO_2 grain boundary, since intergranular insulating layer separating two SnO_2 grain was observed. The negative surface charge at the grain boundary interface is compensated by the positive charge in the grain depletion layer on both sides of interface [9].

In the present work the addition of Fe_2O_3 to the ternary system $SnO_2 \cdot CoO \cdot Nb_2O_5$ was considered aiming to verify the influence of this oxide in the potential barrier formation as well as the microstructure modifications.

2. Experimental procedure

Analytical grades of SnO_2 (Merck), CoO (Riedel), Nb_2O_5 (Aldrich), and Fe_2O_3 (Merck), were used as precursors for processing SnO_2 based ceramics. Varistor compositions powders were prepared by weighting the oxide precursors and using ball mill to mix the oxides. The powders were uniaxial pressed in pellet shapes using a pressure of 75 MPa. The pellets were then isostatically pressed using a pressure of 200 MPa. The samples were then sintered in ambient atmosphere at 1300°C during 2 hours and then were slow cooling down (3°C/min) until ambient temperature. Apparent bulk densities were determined by weighting the samples and measuring the volume by geometric dimensions.

Microstructures were characterized by using a scanning electron microscopy (SEM) (Jeol Model JSM T330A). The samples were ground, polished and thermally etched at 1250°C during 15 min for microstructure revealing. Grain sizes were measured based on the method proposed by Mendelson [11]. The crystalline phases were determined by X-ray diffraction (XRD) using a θ–2θ goniometer (Siemens Model D-5000). The lattice parameters were determined using X-ray diffraction data through the least squares refinement using a computing program.

The samples were ground to reach 1 mm thick with parallel faces and silver electrodes were deposited in these faces for electrical characterization. The electrical voltage as function of electrical current was determined using a voltage source (Tectrol model TCH 3000-2) and measuring the electrical current and voltage by two

digital multimeters (Fluke 8050 A). Then the electric field ($E = V/d$) and current density ($J = I/A$), where d is the sample thickness and A is the sample electrode area, were determined for several applied voltages. The non-linear coefficient (α) was determined by linear regression of the ln E versus ln J curve from 1 mA/cm^2 and the electric field breakdown was determined at this electrical current density.

3. Results and discussions

Fig. 1 show the XRD patterns for the $SnO_2 \cdot CoO \cdot Nb_2O_5$ system with addition of 0.05 or 0.1 mol% of Fe_2O_3. Lattice parameters were determined from these patterns and are listed in Table I and compared with the undoped basic SnO_2 system. Lattice parameters decreased with increasing amount of Fe_2O_3 which imply the formation of solid solution. Both lattice parameters, a and c, decreased due to substitution of Sn^{4+} (ionic radius 0.64 Å) by Fe^{3+} (ionic radius 0.71 Å). XRD patterns of both systems indicated only the SnO_2 crystalline phase indicating solid solution. However dopants concentration used were well bellow the detection limit of XRD.

The addition of Fe_2O_3 in the ternary system did not change significantly the final density of the ceramics sintered in the same conditions, as shown in Table II. However grain size decreased from 8.5 μm in the undoped ternary system to 5.4 μm after doping with 0.05% of Fe_2O_3, indicating that Fe_2O_3 is inhibiting grain growth in this system.

Pianaro *et al.* [7, 8] also observed a similar behavior when the basic SnO_2 varistor ceramics is doped with Cr_2O_3. According to these authors, the Cr_2O_3 should segregate at the grain boundaries, inhibiting then the sintering and grain growth. In the same way Fe_2O_3 should segregate at the grain boundaries inhibiting grain growth during sintering, since the mean grain size decreases from 8.5 μm for the sintered basic ternary system to 5.4 μm for the Fe_2O_3 doped system (Fig. 2). This segregation of iron oxide is due to the low solubility of this oxide in the SnO_2 matrix [12].

As expected the addition of Fe_2O_3 affects the electrical properties of the SnO_2 based varistor. Due to modifications in the microstructure the breakdown electric field increases with the Fe_2O_3 concentration as observed in the Fig. 3 and Table III. This behavior can be explained by the calculated values of the potential barrier per grain (v_b) by using the following expression [13, 14]:

$$E_r = n v_b, \tag{1}$$

being E_r the electric field breakdown and n the number of grains per unit length calculated by:

$$n = \frac{L}{d}, \tag{2}$$

being L the sample thickness and d the mean grain size. The calculated v_b values are shown in Table III and increases with increasing amount of Fe_2O_3 concentration.

TABLE I Lattice parameters of the system $SnO_2 \cdot CoO \cdot Nb_2O_5 \cdot Fe_2O_3$

Mol% of Fe_2O_3	Lattice parameter (Å)		Unit cell volume (Å^3)
	a	c	
0.00	4.738	3.187	71.55
0.05	4.737	3.186	71.49
0.10	4.729	3.183	71.18

TABLE II Relative densities and average grain size for samples sintered 2 h at 1300°C

Composition in mol%	Relative densities (%)	Average grain size (μm)
98.95 SnO_2 + 1.0CoO + 0.05Nb_2O_5	98.0	8.5
98.90 SnO_2 + 1.0CoO + 0.05Nb_2O_5 + 0.05Fe_2O_3	97.6	5.4
98.85 SnO_2 + 1.0CoO + 0.05Nb_2O_5 + 0.1Fe_2O_3	97.7	5.5

TABLE III Effect of dopant concentration on the electric parameters of the system: (98.95 − x) SnO_2 + 1.0CoO + 0.05Nb_2O_5 + $x$$Fe_2O_3$ (all in mol%)

Mol% Fe_2O_3	α	E_r (V/cm)	I_f(A) (1290 V/cm)	V_b (V/barrier)
0.0	8.0	1870	$8.0.10^{-5}$	1.20
0.05	13.0	3185	$3.0.10^{-6}$	1.72
0.10	13.0	4422	$1.8.10^{-7}$	2.43

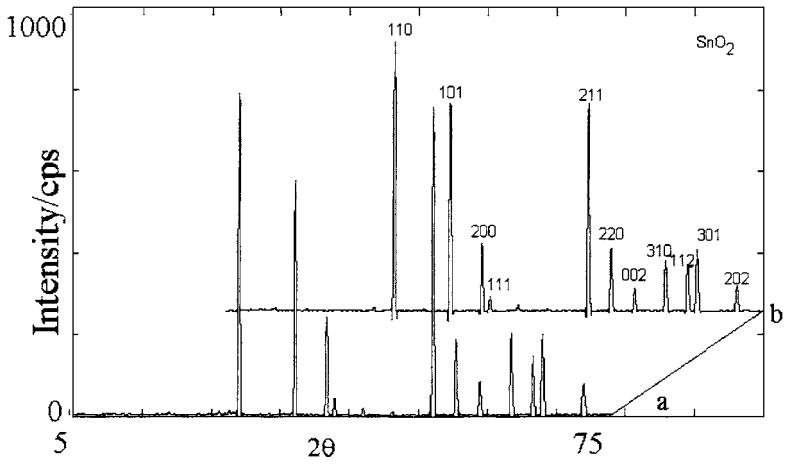

Figure 1 X-ray diffractograms for the (0.9895 − x) SnO_2 + 0.01 CoO + 0.0005 Nb_2O_5 + x Fe_2O_3 system. (a) x = 0.0005 mol%; and (b) x = 0.001 mol%.

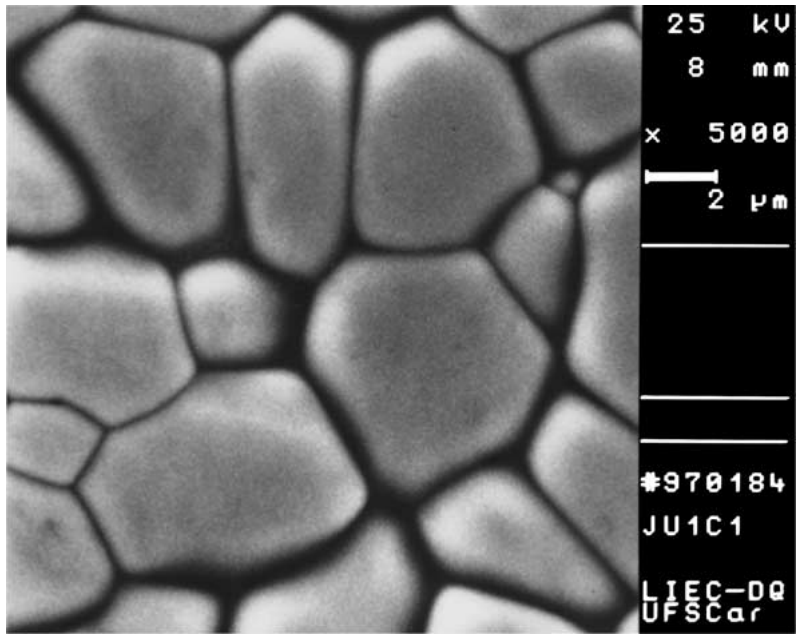

(a)

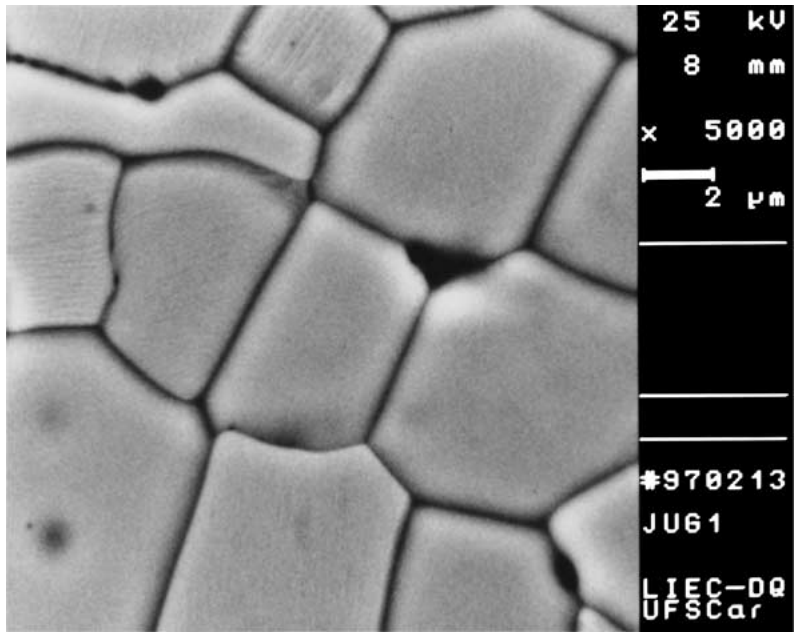

(b)

Figure 2 SEM micrograph of the 0.989 $SnO_2 + 0.01$ CoO + 0.0005 $Nb_2O_5 + 0.0005$ Fe_2O_3 system sintered at 1300°C for 2 h. (b) SEM micrograph of the 0.9885 $SnO_2 + 0.01$ CoO + 0.0005 $Nb_2O_5 + 0.001$ Fe_2O_3 system sintered at 1300°C for 2 h. The sample surface was thermally etched at 1250°C for 15 min.

As proposed by Pianaro *et al.* [4] the electrical conduction for low applied electric field for the $SnO_2 \cdot CoO \cdot Nb_2O_5$ system can be associated to the thermionic emission of the Schottky type. For these varistor systems containing only small additions of Fe_2O_3 the same model for the thermionic emission was considered. In this type of emission, the current density depends on the temperature, according to the following expression [15]:

$$J = J_0 \exp\left(\frac{E_a}{kT}\right), \tag{3}$$

where J_0 is a constant, E_a is the activation energy for an electron jump, k is the Boltzmann constant and T is the absolute temperature. Considering that the potential barrier are of Schottky type separated by thin film and that the conduction mechanism is by thermionic emission, the current density is related to the electric field, E, by the following equation [16]:

$$J_S = A^* T^2 \exp\left(\frac{\phi_B - \beta E^{1/2}}{kT}\right), \tag{4}$$

where A^* is the Richardson constant, ϕ_B is the potential barrier height at the interface, E is the applied electric field and β is related with the potential barrier width by the relation:

$$\beta = \left(\frac{1}{nw}\right)^{1/2} \left(\frac{e^3}{4\pi\varepsilon_0\varepsilon_r}\right)^{1/2}, \tag{5}$$

where n is the number of grains per unit length, ω is the depletion layer width (potential barrier width); e, ε_0 and

TABLE IV Effect of dopant concentration on the potential barrier height (ϕ_B) and width (β) for the system: $(98.95-x)$ $SnO_2 + 1.0\,CoO + 0.05\,Nb_2O_5 + x Fe_2O_3$ (all in mol%)

Mol% Fe_2O_3	ϕ_B (eV)	$\beta \cdot 10^{-3}$ ($V^{-1/2}$ $cm^{1/2}$)
0.0	0.49	7.10
0.05	0.97	4.46
0.10	0.99	3.63

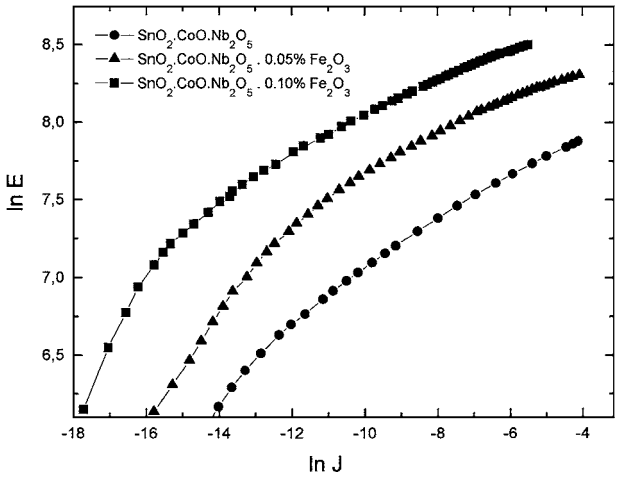

Figure 3 Ln E versus ln J characteristic curves for the SnO_2 based varistor systems sintered at 1300°C for 2 h. (a) 0.9895 $SnO_2 + 0.01$ $CoO + 0.0005$ Nb_2O_5, (b) 0.989 $SnO_2 + 0.01$ $CoO + 0.0005$ $Nb_2O_5 + 0.0005$ Fe_2O_3, (c) 0.9885 $SnO_2 + 0.01$ $CoO + 0.0005$ $Nb_2O_5 + 0.001$ Fe_2O_3.

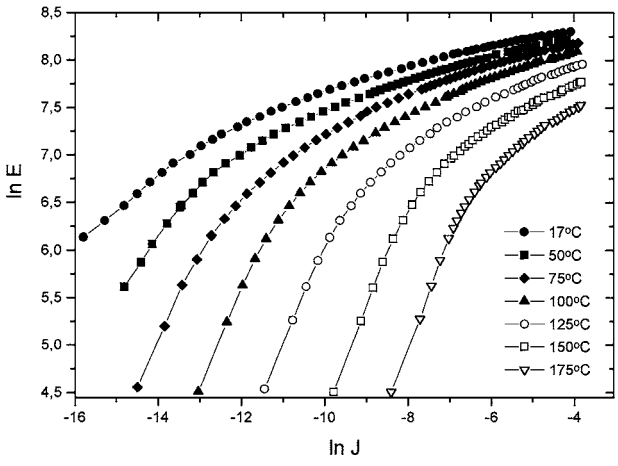

Figure 4 Ln E versus ln J characteristic curves for the SnO_2 based varistor systems sintered at 1300°C for 2 h and measured at different temperatures: (a) 0.989 $SnO_2 + 0.01$ $CoO + 0.0005$ $Nb_2O_5 + 0.0005$ Fe_2O_3, (b) 0.9885 $SnO_2 + 0.01$ $CoO + 0.0005$ $Nb_2O_5 + 0.001$ Fe_2O_3.

ε_r are the electronic charge, vacuum electric permissivity and material electric permissivity respectively.

The plot of ln E versus ln J for temperatures ranging from 16 to 175°C is shown in Fig. 4. As observed in this plot the leakage current increase with increasing temperatures. The thermionic emission can be characterized by plotting ln J versus $E^{1/2}$ and considering the ohmic region of the curves a linear plot is observed (Fig. 5). By extrapolating the curves to $E = 0$, values $J_s(0)$ versus $1/T$ gives value of the potential barrier height (ϕ_B) (Fig. 6). Values for (ϕ_B) and β for the $SnO_2 \cdot CoO \cdot Nb_2O_5$ system and with 0.05 and 0.10 mol% of Fe_2O_3 are shown in Table IV. These values varies from 0.49 to 0.97 and 0.99 eV, while β decreases substantially which represents a increase in the potential barrier width ($\omega \propto \beta^2$).

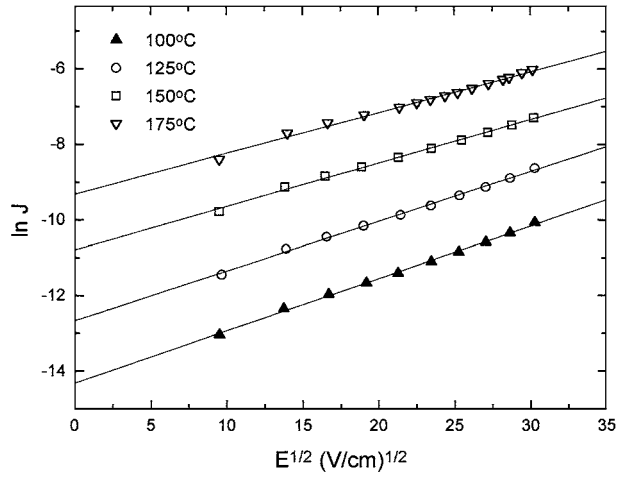

Figure 5 Ln J versus $E^{1/2}$ characteristic curves for the SnO_2 based varistor systems sintered at 1300°C for 2 h and measured at different temperatures: (a) 0.989 $SnO_2 + 0.01$ $CoO + 0.0005$ $Nb_2O_5 + 0.0005$ Fe_2O_3, (b) 0.9885 $SnO_2 + 0.01$ $CoO + 0.0005$ $Nb_2O_5 + 0.001$ Fe_2O_3.

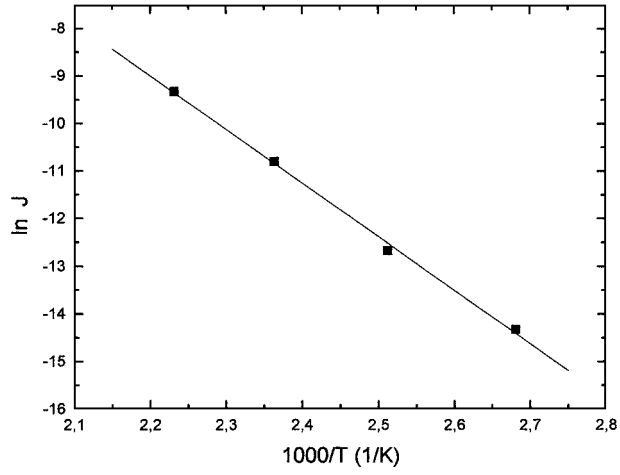

Figure 6 Ln J versus $1/T$ characteristic curves for the SnO_2 based varistor systems sintered at 1300°C for 2 h and measured at different temperatures: (a) 0.989 $SnO_2 + 0.01$ $CoO + 0.0005$ $Nb_2O_5 + 0.0005$ Fe_2O_3, (b) 0.9885 $SnO_2 + 0.01$ $CoO + 0.0005$ $Nb_2O_5 + 0.001$ Fe_2O_3.

This behavior can be explained by the creation of point defects due to the solid solution of Fe_2O_3, in addition to the solid solution of Nb_2O_5 and CoO in the SnO_2 [4–8, 17, 18], according to the following equations:

$$Fe_2O_3 \xrightarrow{SnO_2} 2Fe'_{Sn} + V^{\bullet\bullet}_O + 3O^x_O, \quad (6)$$

$$2Nb_2O_5 \xrightarrow{SnO_2} 4Nb^{\bullet}_{Sn} + V^{\prime\prime\prime\prime}_{Sn} + 10O^x_O, \quad (7)$$

$$CoO_3 \xrightarrow{SnO_2} Co''_{Sn} + V^{\bullet\bullet}_O + O^x_O. \quad (8)$$

The increase in the potential barrier height and in the potential barrier width are associated to the increase of both, N_s and N_d due to the segregation of Fe_2O_3 next to the grain boundary as well as the creation of positive defect in the depletion layer ($V^{\bullet\bullet}_O$) and negative defects at the interface (Fe'_{Sn}). After the adsorption of oxygen at interface there is a transfer of negative charges from

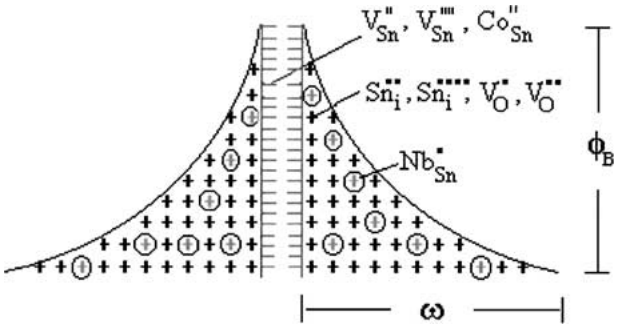

Figure 7 Atomic defect model proposed to explain the potential barrier formation at the grain boundaries of SnO_2 based varistor systems.

Fe'_{Sn} and other negative species to the adsorbed oxygen which increase N_s. then the increase of potential barrier can be associated to the increase of effective surface states (N_s) according to the following equation:

$$\phi = \frac{e^2 N_s}{2_o \varepsilon_r N_d}. \tag{9}$$

Considering the SnO_2 varistor microstructure, a Schottky type electrical barrier can be ascribed to be most likely barrier at the SnO_2 grain boundary, since no intergranular insulating layer separating two SnO_2 grains as observed. The negative surface charge at the grain boundary interface is compensated by the positive charge in the depletion layer in the grain on both sides of the interface [9]. Based on previous studies, Gupta and Carlson developed a grain boundary defect model comprising the Schottky barrier [10]. In an attempt to explain the grain boundary barrier formation in SnO_2 varistor, an analogy to this model can be considered, as shown in Fig. 7. In our model, the intrinsic SnO_2 defects (V''''_{Sn}, $V^{\bullet\bullet}_O$) and extrinsic defects created by the dopants CoO, Fe_2O_3 and Nb_2O_5 should be responsible for the grain boundary electrical barrier formation. These dopants form a solid solution with the SnO_2 at high temperatures and create defects near the grain boundary according to Equations 3 to 5.

In Fig. 7, positively charged donors ($V^{\bullet\bullet}_O$, $Nb^{\bullet}_{Sn}$) extending from both sides of grain boundary are compensated by negative charged acceptors (V''''_{Sn}, V''_{Sn}, Co'_{Sn}, Co''_{Sn}, Fe'_{Sn}) at the grain boundary interface. The oxygen can be adsorbed at the interface and react with negative defects according to the following equations [18–20]:

$$O_2 \rightarrow O^x_{2(ad)}, \tag{10}$$

$$V''''_{Sn} + 4O^x_{2(ad)} \rightarrow 4O'_{2(ad)} + V^x_{Sn}, \tag{11}$$

$$V''''_{Sn} + 2O^x_{2(ad)} \rightarrow V''_{Sn} + 2O'_{2(ad)}, \tag{12}$$

$$V''_{Sn} + 2O'_{2(ad)} \rightarrow V^x_{Sn} + 4O'_{2(ad)}, \tag{13}$$

$$Co''_{Sn} + 2O^x_{2(ad)} \rightarrow 2O'_{2(ad)} + Co^x_{Sn}, \tag{14}$$

$$Fe'_{Sn} + O^x_{2(ad)} \rightarrow O'_{2(ad)} + Fe^x_{Sn}, \tag{15}$$

$$Fe'_{Sn} + O'_{2(ad)} \rightarrow Fe^x_{Sn} + 2O'_{ad}. \tag{16}$$

The adsorbed oxygen at the grain boundary captures electrons from negatively charged defects at the grain boundary and stays at the interface. This effect was confirmed by impedance analysis [21].

4. Conclusions

Additions of 0.05 e 0.10% of Fe_2O_3 (in mol%) to the $SnO_2 \cdot CoO \cdot Nb_2O_5$ system lead to decrease of both: mean grain size and leakage current as well as lead to increase of the non-linear coefficient and breakdown electric field. The potential barrier height are 0.97 and 0.99 eV respectively. The non-linear behavior of these ceramics can be explained by the formation of atomic defects in the depletion layer ($V^{\bullet\bullet}_O$, $Nb^{\bullet}_{Sn}$) and at interface (V''''_{Sn}, V''_{Sn}, Co'_{Sn}, Co''_{Sn}, Fe'_{Sn}). Moreover, the adsorbed oxygen at grain boundaries captures electrons from negatively charged defects at the grain boundary and is the major responsible for the negative charge density at the interface.

Acknowledgements

This work received financial support from Brazilian Research agencies FAPESP/CEPID and CNPq/PRONEX.

References

1. Z. M. JARZEBSKI and J. P. MARTON, *J. Electrochem. Soc.* **123** (1976) 299C.
2. J. A. VARELA, E. LONGO, N. BARELLI, A. S. TANAKA and W. A. MARIANO, *Cerâmica* **31** (1985) 241.
3. J. A. VARELA, O. J. WHITTEMORE and E. LONGO, *Ceram. Inter.* **16** (1990) 177.
4. S. A. PIANARO, P. R. BUENO, P. OLIVI, E. LONGO and J. A. VARELA, *J. Mater. Sci. Lett.* **16** (1997) 634.
5. A. C. ANTUNES, S. R. M. ANTUNES, M. A. ROCHA, S. A. PIANARO, E. LONGO and J. A. VARELA, *J. Sci. Letter* **17** (1998) 577.
6. A. C. ANTUNES, S. R. M. ANTUNES, S. A. PIANARO, E. LONGO and J. A. VARELA, *J. Mater. Sci.* **35** (2000) 1453.
7. S. A. PIANARO, P. R. BUENO, P. OLIVI, E. LONGO and J. A. VARELA, *J. Sci. Mater. Elect.* **9** (1998) 159.
8. S. A. PIANARO, P. R. BUENO, E. LONGO and J. A. VARELA, *Ceram. Inter.* **25** (1991) 1.
9. T. K. GUPTA, *J. Amer. Ceram. Soc.* **73** (1990) 1817.
10. T. G. GUPTA and W. G. CARLSON, *J. Mater. Sci.* **20** (1985) 3487.
11. M. I. MENDELSON, *J. Amer. Ceram. Soc.* **52** (1969) 443.
12. S. MUSIC, S. POPOVIC, S. M. METIKO-HUKOVIC and G. VOZDIC, *J. Mater. Sci. Lett.* **10** (1991) 197.
13. J. F. MCALER, P. T. MOSELEY, J. O. W. NORRIS and D. E. WILLIANS, *J. Chem. Soc. Faraday Trans.* **83** (1987) 1323.
14. J. WONG, *J. Appl. Phys.* **47**(11) (1976) 4971.
15. S. M. SZE, "Physics of Semiconductor Devices" (Wiley, New York, 1985).
16. K. EDA, *J. Appl. Phys.* **49** (1987) 2964.
17. J. A. VARELA, J. A. CERRI, E. R. LEITE, E. LONGO, M. SHAMSUZZOHA and R. C. BRADT, *Ceram. Inter.* **25** (1999) 253.
18. J. D. SANTOS, E. LONGO, E. R. LEITE and J. A. VARELA, *J. Mater. Res.* **13** (1998) 5.
19. E. R. LEITE, A. M. NASCIMENTO, P. R. BUENO, E. LONGO and J. A. VARELA, *J. Mater. Sci: Mater Elect.* **10** (1999) 1.
20. E. R. LEITE, J. A. VARELA and E. LONGO, *J. Mater. Sci.* **27** (1992) 5325.
21. P. R. BUENO, S. A. PIANARO, E. C. PEREIRA, L. O. S. BULHÕES, E. LONGO and J. A. VARELA, *J. Appl. Phys.* **84**(7) (1998) 159.

Received 20 September 2001
and accepted 30 January 2002